NASA Technical Memorandum 110438

NASA Ames Laminar Flow Supersonic Wind Tunnel (LFSWT) Tests of a 10° Cone at Mach 1.6

Stephen W. D. Wolf, MCAT, Inc., San Jose, California
James A. Laub, Ames Research Center, Moffett Field, California

March 1997

National Aeronautics and
Space Administration

Ames Research Center
Moffett Field, California 94035-1000

Contents

NASA Ames Laminar Flow Supersonic Wind Tunnel (LFSWT) Tests of a 10° Cone at Mach 1.6

STEPHEN W. D. WOLF* AND JAMES A. LAUB

Ames Research Center

Summary

This work is part of the ongoing qualification of the NASA Ames Laminar Flow Supersonic Wind Tunnel (LFSWT) as a low-disturbance (quiet) facility suitable for transition research. A 10° cone was tested over a range of unit Reynolds numbers (Re = 2.8 to 3.8 million per foot (9.2 to 12.5 million per meter)) and angles of incidence (0° to 10°) at Mach 1.6. The location of boundary layer transition along the cone was measured primarily from surface temperature distributions, with oil flow interferometry and Schlieren flow visualization providing confirmation measurements. With the LFSWT in its normal quiet operating mode, no transition was detected on the cone in the test core, over the Reynolds number range tested at zero incidence and yaw. Increasing the pressure disturbance levels in the LFSWT test section by a factor of five caused transition onset on the cone within the test core, at zero incidence and yaw. When operating the LFSWT in its normal quiet mode, transition could only be detected in the test core when high angles of incidence (>5°) for cones were set. Transition due to elevated pressure disturbances (Tollmien-Schlichting) and surface trips produced a skin temperature rise of order 4° F (2.2° C). Transition due to cross flows on the leeward side of the cone at incidence produced a smaller initial temperature rise of only order 2.5° F (1.4° C), which indicates a slower transition process. We can conclude that these cone tests add further proof that the LFSWT test core is normally low-disturbance (pressure fluctuations > 0.1%), as found by associated direct flow quality measurements discussed in this report. Furthermore, in a quiet test environment, the skin temperature rise is sensitive to the type of dominant instability causing transition. The testing of a cone in the LFSWT provides an excellent experiment for the development of advanced transition detection techniques.

1. Introduction

The 10° cone test is a widely accepted indirect measurement of flow quality in wind tunnels and the atmosphere (a pseudo-standard it might be said). This test is concerned with the location of transition along the surface of the cone. Unfortunately, transition is not a function of flow disturbances alone, but also the cone's geometry, surface finish, and orientation to the flow. A large database already exists on the measured locations of transition along numerous cones in quiet and noisy flow fields. A major part of this database was amassed by the exhaustive efforts of Dougherty and Fisher (refs. 1–3) who effectively isolated flow disturbances as the only influence on the cone transition. This was achieved by personally setting up and testing the exact same model in different test environments, both in flight and ground test facilities.

The 10° cone test provided an opportunity to match the unique ground test Mach 1.6 flow field of the LFSWT against the quiescent atmosphere at HSCT cruise altitudes, and the flow fields of production-type supersonic wind tunnels. In addition, the 10° cone test provides a near ideal setup for the development of transition detection techniques. These techniques are required for tests of more complex aerodynamic surfaces, such as those found on a swept wing.

The published cone database (at near zero yaw and incidence) has been summarized in figure 1 for the Mach 1.6 test conditions found in the LFSWT. The location of transition onset on a 10° cone, in both flight and production wind tunnels, is greater than 10 inches (25.4 cm) from the tip over the unit Reynolds number (Re) range from 2 to 4 million per foot (6.6 to 13 million per meter). At Mach 1.6 in the LFSWT (ref. 4), the bow shock reflected from the floor and ceiling was expected to impinge on the cone, and trip the boundary layer, about 8 inches (20.3 cm) from the tip. The downstream extent of the LFSWT quiet test core is fixed by this reflected bow shock. Consequently, these tests were planned with the expectation that transition on the clean cone (at zero yaw and incidence) would only occur due to the reflected-shock/boundary-layer interaction.

Interestingly, the blockage of the 15 inch (38.1 cm) long cone tested in the LFSWT is 4.2%, as compared to a maximum of 2% in similar production wind tunnel tests

*MCAT, Inc., 3933 Blue Gum Dr., San Jose, CA 95127.

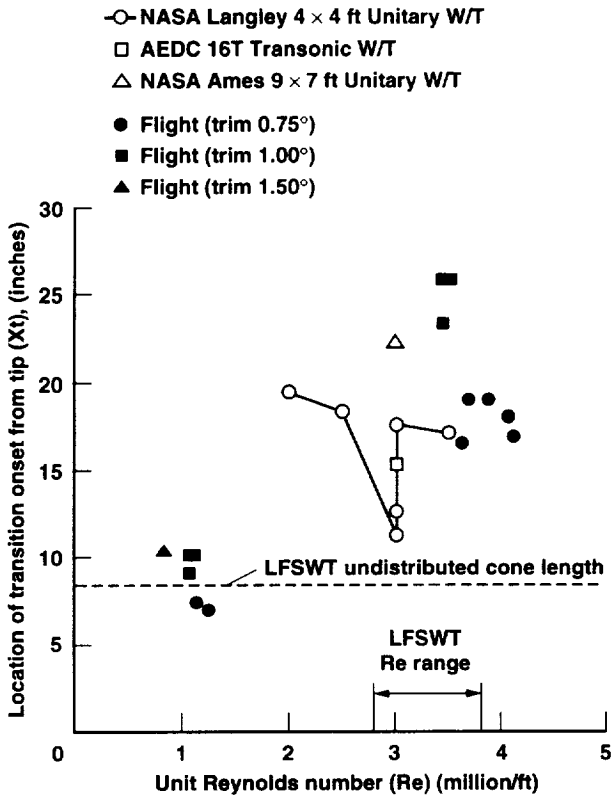

Figure 1. Comparison of flight test and wind tunnel 10° cone transition data. Cone length = 44.5 inches (1.13 m); Mach 1.6 (approx.); transition free; near zero yaw and incidence. (Data extracted from NASA TP-1971.)

(where the cone was 44.5 inches (1.13 meters) in length). Consequently, the LFSWT cone test was expected to be more sensitive to the state of the wall boundary layers, because the test section walls were 8 times closer to the cone than in other wind tunnel tests. Hence in the LFSWT tests, radiated noise from the test section walls would be less attenuated at the cone location (ref. 5).

To study and calibrate different transition detection techniques in the LFSWT, transition was induced on the cone within the test core. This was achieved by applying trip tape as surface roughness, inducing cross flows with angle of attack, and increasing free stream turbulence by tripping the tunnel wall boundary layers.

Transition on the cone was primarily detected by the different adiabatic skin temperatures associated with laminar and turbulent boundary layers. The temperature recovery properties of laminar and turbulent flow are such that the skin temperatures of the cone, for a given total temperature, vary depending on the boundary layer state (turbulent flow induces warmer skin temperatures). It was estimated that the peak temperature rise across the transition front should be order 8° F (4.4° C) based on published temperature recovery factors of 85% for laminar flow and 90% for transitional flow. Other transition detection techniques using Schlieren flow visualization, and oil flow interferometry were also used.

This report summarizes the cone test results from the LFSWT. The intent here is to document our measurements as a basis for further analyses and tests. This data set is unique because the flow quality in the LFSWT has been studied extensively (refs. 4, 6, and 7), so the free stream disturbances (boundary conditions) are much better understood. Furthermore, data are presented to show the receptivity of the cone boundary layer to different free stream disturbances and cross-flow instabilities.

2. Model and Tunnel Description

2.1 10° Cone

The 10° cone (5° half-angle) used in these tests was loaned from NASA Langley Research Center. A new cone tip had to be made to replace the original, which had been made blunt. The cone is 15 inches (38.1 cm) long, made from 17-4 stainless steel and is hollow, with a nominal skin thickness of 0.030 inch (0.76 mm). An array of 106 type-K thermocouples was spot welded to the inside surface of the cone skin, equally spaced (0.25 inch (6.35 mm) apart starting 1.5 inches (3.8 cm) from the tip) along two rays, 180° apart. These rays were positioned horizontally in the tunnel for the tests described here.

In preparation for the LFSWT tests, the influences of the cone surface finish and geometry on transition location were minimized. Our intent here was to provide an objective comparison of the LFSWT cone data with other published results. The surface quality of the cone was maintained in a state of high polish with a 2L (2 micro-inch (0.05 micron)) finish. Also, the nose tip was validated as concentric with the body, with a sharpness defined as a less than 0.001 inch (0.025 mm) tip flat radius. The cone was held precisely in all three planes, to avoid yaw errors which would otherwise be introduced by angle of attack adjustments. The position of the cone in the test section (as shown in fig. 2) was validated to within 0.002 inch (0.051 mm), which corresponds to an incidence accuracy of 0.015°.

A simple design was chosen for the cone support using an existing LFSWT ceiling window blank with a turntable (ref. 4), as shown in figure 2. The design includes a vertical support with a 90° knuckle joint, and a horizontal support attaching to the base-plate of the cone. The vertical support was mounted in the turntable for angle

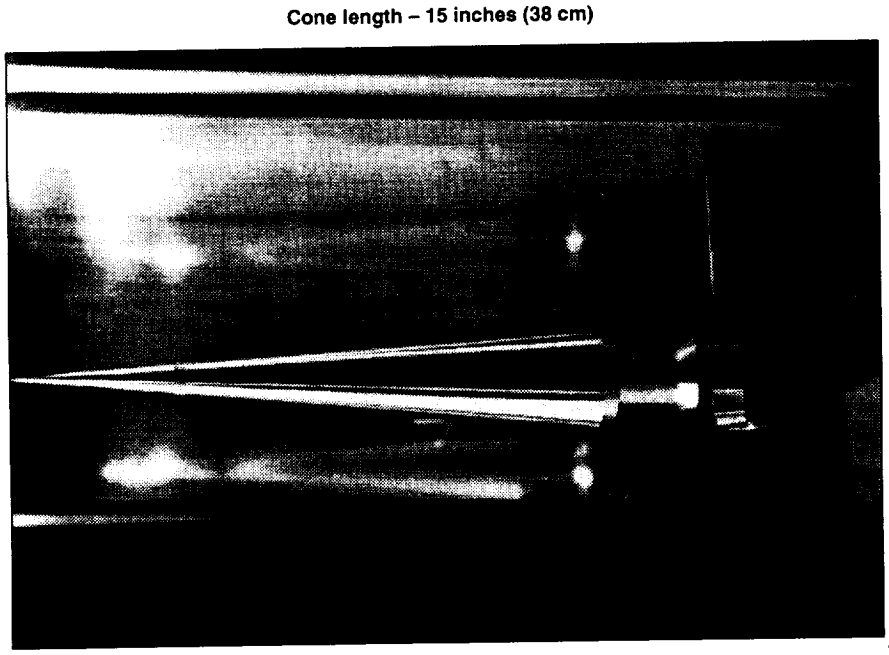

Figure 2(a). The 10° cone mounted in the LFSWT with trip tape fitted. Cone length = 15 inches (38 cm).

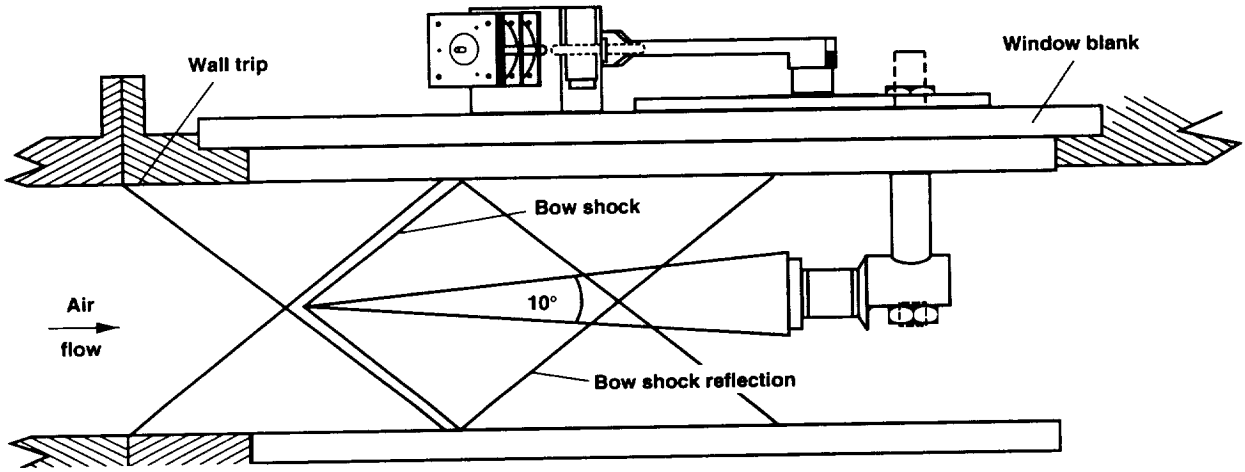

Figure 2(b). Schematic of 10° cone flow field in the LFSWT test section. (Some shock and Mach wave reflections removed for clarity.)

of attack control. The support was made hollow to allow cone instrumentation wiring to be brought out of the tunnel. Emphasis was placed on accurately holding the cone, and on support stiffness to minimize vibration. Predicted natural frequencies of the support with three different horizontal lengths were compared with measured test section vibration spectra, to select the support length that showed the least possibility of vibration excitation by the tunnel. The shortest horizontal support was chosen to give the best vibration protection.

2.2 LFSWT Overview

The LFSWT has an 8 inch (20.32 cm) high, 16 inch (40.64 cm) wide, and 32 inch (81.28 cm) long test section, designed with optical access from all four sides.

Over 60% of the test section surface area can be fitted with windows. The test section was sized for continuous operation with mass flows up to 27 lb/sec (12.2 kg/sec). The distinctive aerodynamic features of the LFSWT are a low-disturbance settling chamber, laminar boundary layers on the nozzle and test section walls, steady supersonic diffuser flow, and low structural vibration of the nozzle and test section walls. Furthermore, the tunnel is designed to run continuously at Mach 1.6 with unusually low stagnation pressures, with uniquely low compression ratios (less than unity). The tunnel achieves this capability by utilizing a unique two-stage injector drive system (ref. 4).

The test section is cantilevered from the exit plane of the supersonic nozzle block. All joints exposed to the flow were hand finished with no forward facing steps permitted. Nevertheless, weak Mach lines were detected by Schlieren visualization coming from the upstream joints (as shown later). The test section and nozzle flow surfaces were maintained in a mirror-like state with a 10L (10 microinch (0.25 micron)) finish to promote laminar boundary layers. Specific details about each component of the LFSWT can be found in reference 4.

3. Tunnel Flow Quality

While the cone test serves as an indirect measure of flow quality, it is extremely useful to match this measure against direct flow quality measurements. In the LFSWT, extensive flow measurements have been made with an array of instrumentation (refs. 6 and 7).

In the test section, we can summarize the centerline total pressure disturbances (Prms/Pt) as shown in figure 3, over the range of stagnation pressure (Po). The measurements were made at 3 streamwise locations in the test section (X = 27.35 corresponds to the test section entrance, and is the distance in inches from the nozzle throat). This data was acquired with an XCS-093 transducer (15 psia (1.03 bar) range) over a 0.25k to 50k bandwidth (refs. 6 and 7). The wind-off noise was subtracted from the wind-on signal, and an in situ transducer calibration using steady state pressures was run in parallel with rms data acquisition. A full description of our data acquisition system can be found in references 6 and 7.

A comparison between pressure transducer signal spectra for the maximum and minimum pressure disturbances recorded is shown in figure 4. There was a broadband increase of disturbances associated with an increase of Po (hence tunnel mass flow), that was independent of streamwise position. Spanwise variation of the pressure disturbances is contained within noise spikes at frequencies below 10 kHz. These noise spikes (with even larger

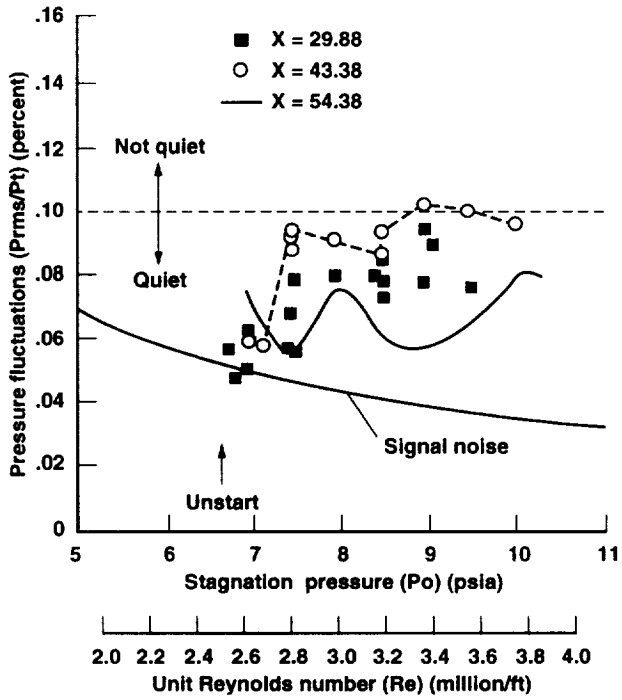

Figure 3. Variation of pressure fluctuations with unit Reynolds number, along the test section. Tunnel centerline, XCS-093 transducer; 0.25–50 kHZ bandwidth.

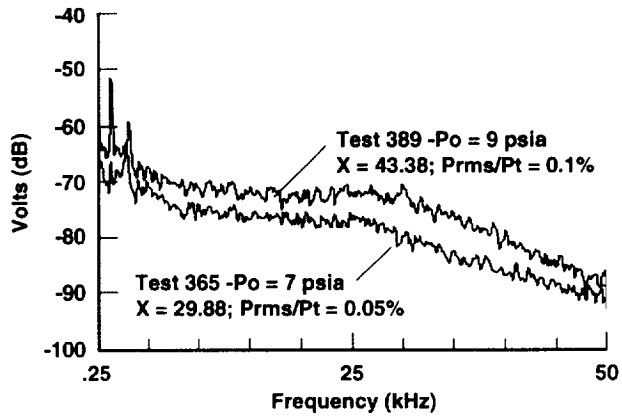

Figure 4. Comparison of maximum and minimum pressure fluctuation spectra measured in the test section. Tunnel centerline; XCS-093 transducer.

amplitude than in these cone tests) have not been observed to affect the state of the boundary layers in the tunnel. The tunnel disturbances actually originate in the air inlet system to the tunnel. The disturbances are temporal, and are dependent on mass flow and stagnation temperature (To), so flow quality measurements are required on a continual basis. The measurements presented here are those taken before and after the actual

cone tests, to provide the best assessment of flow quality during the cone tests. Ideally, some measurement of flow quality should be made in parallel with each transition experiment in the LFSWT.

During the cone tests, the pressure disturbances in the LFSWT test section were increased by tripping the wall boundary layers at the test section entrance. An 0.018 inch (0.457 mm) high strip of 80-grit sandpaper, 0.25 inch (6.35 mm) wide, was glued around the entire circumference of the test section entrance. The leading edge of the wall trip was 5.187 inches (13.2 cm) upstream of the cone tip, and the associated Mach lines crossed 0.27 inch (6.86 mm) ahead of the cone tip, as shown in the Schlieren picture in figures 2 and 5. The pressure disturbances in the test section associated with tripped wall boundary layers are about 0.25%, for the bandwidth 0.25 to 50 kHz, as shown in figure 6 (ref. 4). This increased level of disturbances is up to five times greater than in normal operation. The tripped boundary layer generates increased pressure fluctuations over the entire bandwidth, as shown in Figure 7 for one typical case at Po = 7 psia (0.48 bar). This finding is consistent with the tunnel wall boundary layers being turbulent with the trip fitted.

A five-hole probe was traversed about the test section to measure steady flow parameters. We measured a maximum Mach number deviation of 0.003, with a maximum flow angle standard deviation of 0.07° in the vertical direction, and 0.05° in the horizontal direction. These deviations are within current flow standards for supersonic wind tunnels (ref. 8).

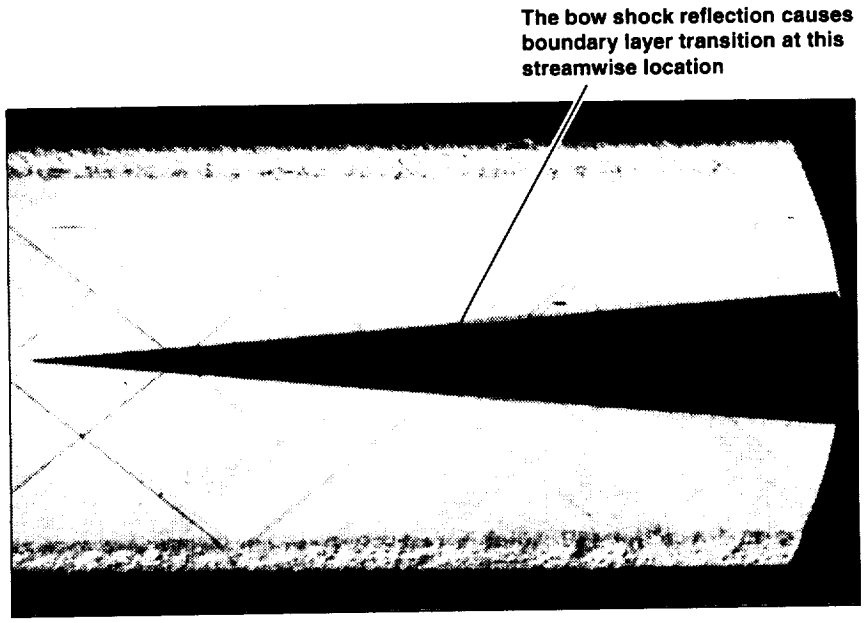

Weak 2-D Mach line disturbances (integrated across the test section width) originate and reflect from the tunnel walls with no apparent effect on the transition process. Thick thermal layers can be seen on the floor and ceiling, due to the hot walls of the settling chamber and test section relative to the flow.

Figure 5. Schlieren flow visualization of the 10° cone test in the LFSWT. Mach 1.58; Po ≈ 7.5 psia (0.52 bar); transition free.

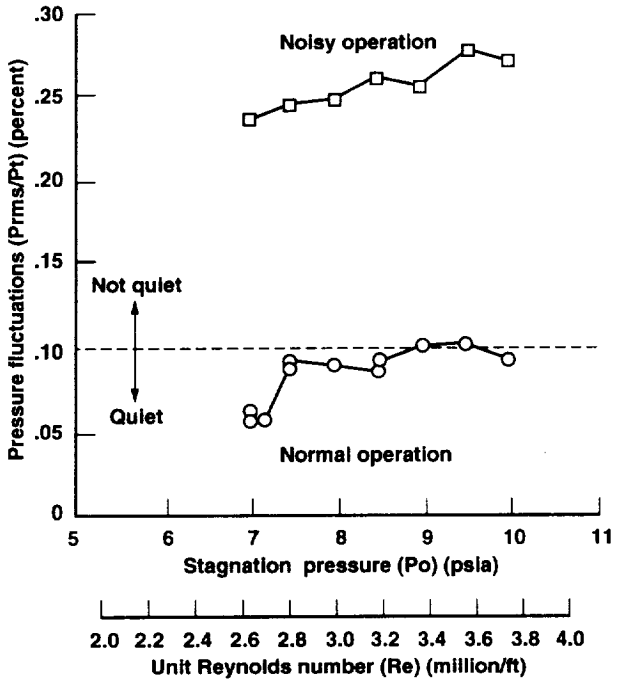

Figure 6. Test section pressure fluctuations with and without boundary layer trips on the tunnel walls. Tunnel centerline; X = 43.38; XCS-093 transducer; 0.2–50 kHz bandwidth.

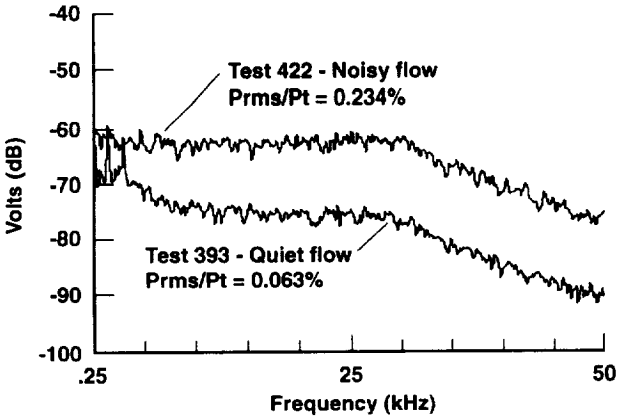

Figure 7. Comparison of pressure fluctuation spectra at the same location and test conditions, with and without boundary layer trips fitted to the tunnel walls. Tunnel centerline; X = 43.38; XCS-093 transducer; Po = 7 psia.

4. Transition Detection

4.1 Skin Temperatures

For each cone test, 64 type-K thermocouples were connected to two ComputerBoards EXP-32 multiplexer boards. Each board was used to multiplex 32 thermocouple inputs to two A/D channels on a ComputerBoards CIO-AD16 12-bit A/D board internally mounted in a PC. Each multiplexer board provided a cold junction temperature. Custom software (written in QuickBASIC using a ComputerBoards library) was used to acquire the temperature data. A total of 1000 samples (acquired at 2.5 kHz) were averaged for each recorded temperature. Signal gain was set to 100 to achieve reasonable signal stability, which gave a 0.9° F (0.5° C) per bit resolution typical of thermocouple measurements.

During initial cone tests, we observed a lack of accuracy and repeatability in the raw skin temperatures. The multiplexer boards were then housed in a thermally isolating box, to minimize differential drifting of the cold junction temperatures. Also, by experimentation, an acquisition procedure was developed to minimize temperature offsets between A/D channels. Typically, a test would commence with the adjustment of the reference temperatures (one per data channel) from thermocouples placed in an ice bath. Next, the wind-off temperatures were taken (assuming the model temperature was ambient and uniform), then the model was allowed to cold soak during the first 20 minutes of each tunnel run (since the LFSWT always operates at cold stagnation temperatures below freezing). Measurements were made at each test condition with no specific time delay, because of the observed fast response of the thermocouples.

Data reduction involved the correction for wind-off temperature variations for each thermocouple, and the removal of variations of the overall skin temperatures due to stagnation temperature (To) drift between runs. We observed a thermal lag between the To measurement in the settling chamber and the cone temperatures. The To had the slowest response, so normalizing the temperatures by calculating temperature recovery factors did not collapse the data sets. Consequently, we decided to consider temperature variations relative to the most upstream thermocouple, 1.5 inches (3.8 cm) from the cone tip. Since the nose mass is small, the most upstream thermocouple is the most sensitive measurement of the free stream temperature. This data reduction procedure collapses different data sets together, and yielded good data repeatability (for thermocouples), of order ±1° F (±0.55° C), as shown later.

4.2 Oil Flow Interferometry

An oil flow interferometry technique was used to measure skin friction at discrete points on the cone. The technique, modernized and performed by Zilliac (ref. 9) from the NASA Ames Fluid Mechanics Laboratory, employs interferometry to measure the slope of an oil flow on a reflective surface. Since the flow of the oil is related to the viscosity and shear, the history of temperature and dynamic pressure must be known from tunnel start-up to the moment the oil thickness is measured. For these cone tests, the oil viscosity of 500 centiStokes was used in laminar flow regions, and 2000 centiStokes was used in the turbulent regions, to provide reasonable lengths for the oil flows. Furthermore, the skin friction on a given oil flow must be either laminar or turbulent through the history period. Hence, the technique has limited applicability to the actual detection of transition, and is better suited to the confirmation of it. The accuracy of this oil flow interferometry technique is thought to be better than the 20% claimed by other shear stress measurement techniques, using surface balances.

4.3 Schlieren Flow Visualization

A conventional 2-mirror Toepler Schlieren system was used to confirm boundary layer transition on the cone due to the impinging bow shock reflection (as shown in fig. 5). The small boundary layers observed in these cone tests highlight the need for single dimension image magnification if more detail is required. Nevertheless, sufficient detail was available to determine the change in state of the boundary layer. Schlieren quality glass windows were fitted to the LFSWT test section sidewalls for these observations. It should be noted that this flow visualization technique could only be used to observe the vertical rays of the cone (90° from the thermocouple rays).

The Schlieren image in figure 5 also shows the disturbances from trips on the tunnel walls, and weak Mach wave disturbances from hand-finished joints in the test section. These disturbances are integrated across the test section width and had no effect on cone measurements. Interestingly, spatially uniform, thick thermal layers are present above and below the floor and ceiling of the test section respectively. These layers originate in the settling chamber due to the relatively hot walls of the tunnel compared to the flow. Wall trips are fitted in this instance, so the wall boundary layers are turbulent. The wall boundary layers have been probed, and are thought to be considerably thinner with displacement thicknesses of the order 0.1 inch (2.54 mm).

5. Results

The LFSWT cone tests consisted of 93 test points. Data from selected test points plotted in the figures are tabulated in the appendix. The cone was tested at Mach 1.586 over a stagnation pressure (Po) range from 7.5 to 10 psia (0.52 to 0.69 bar), which corresponds to a Re range from 2.8 to 3.8 million per foot (9.2 to 12.5 million per meter). Angle of incidence was varied up to 10° with zero yaw.

Skin temperature variations on the clean cone at zero incidence and yaw are shown in figure 8 over the full LFSWT Re range. A boundary layer trip was fitted by placing a length of tape, 0.011 inch (0.279 mm) high and 0.25 inch (6.35 mm) wide, around the cone, with the leading edge 4.5 inches (11.4 cm) from the tip (as shown in fig. 2). The tripped cone data are shown in figure 9 over the Re Range. Trip-on and trip-off data at zero incidence and yaw are compared in figure 10. Supporting skin friction coefficient data at points along the cone, upstream and downstream of the trip, are summarized in figure 11. A comparison of cone temperatures with quiet and noisy flow (trips fitted on the tunnel walls, as described in sec. 3) is shown in figure 12, over the Re range at zero incidence and yaw. Skin temperatures on a clean cone with quiet flow, and angle of incidence varied up to 10°, are shown in figures 13 and 14.

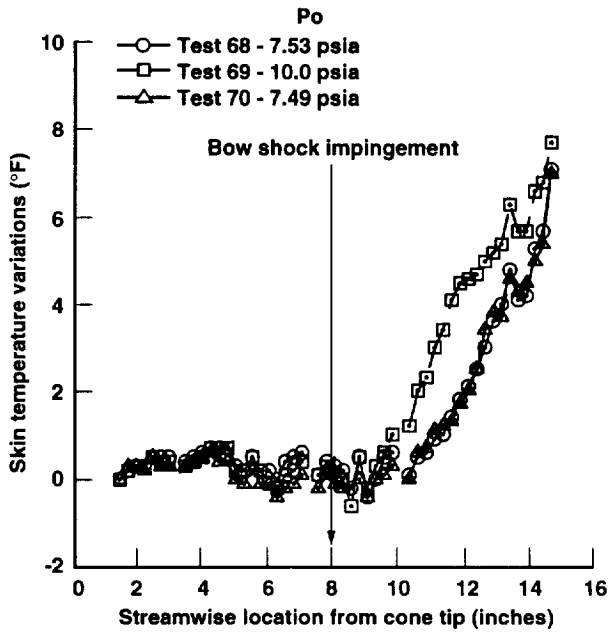

Figure 8. Effect of Reynolds number on 10° cone temperatures with transition free. Cone length = 15 inches (38 cm); Mach 1.586; α = 0°.

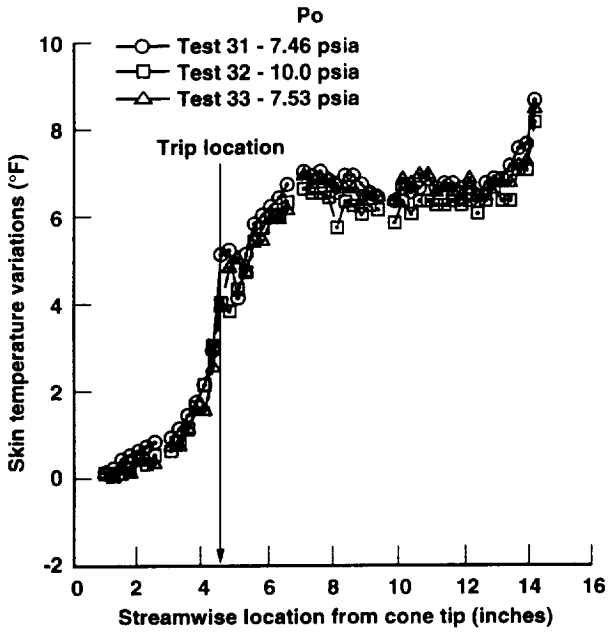

Figure 9. Effect of Reynolds number on 10° cone temperatures with transition fixed. Cone length = 15 inches (38 cm); Mach 1.586; α = 0°.

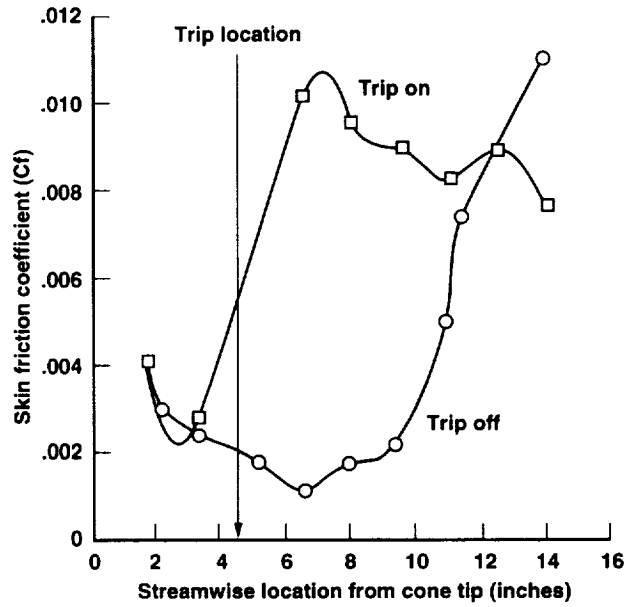

Figure 11. Comparison of 10° cone skin friction coefficients obtained from oil flow interferometry with transition free and fixed at Po = 7.5 psia. Cone length = 15 inches (38 cm); Mach 1.586; α = 0°.

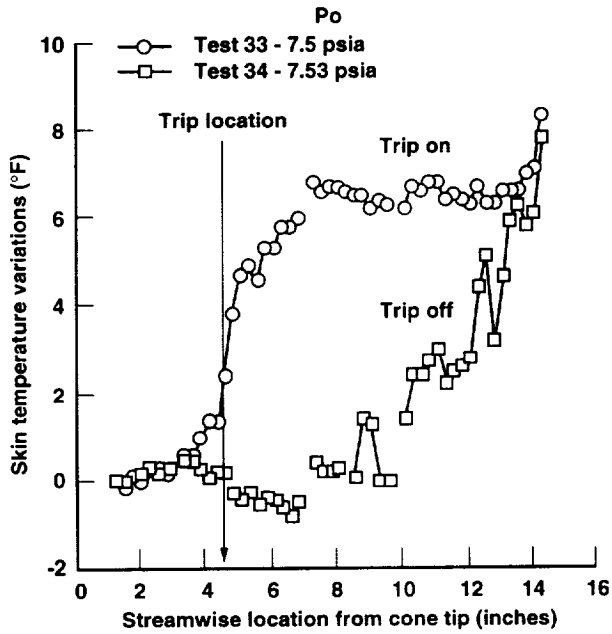

Figure 10. LFSWT 10° cone temperatures with transition free and fixed at Po = 7.5 psia. Cone length = 15 inches (38 cm); Mach 1.586; α = 0°.

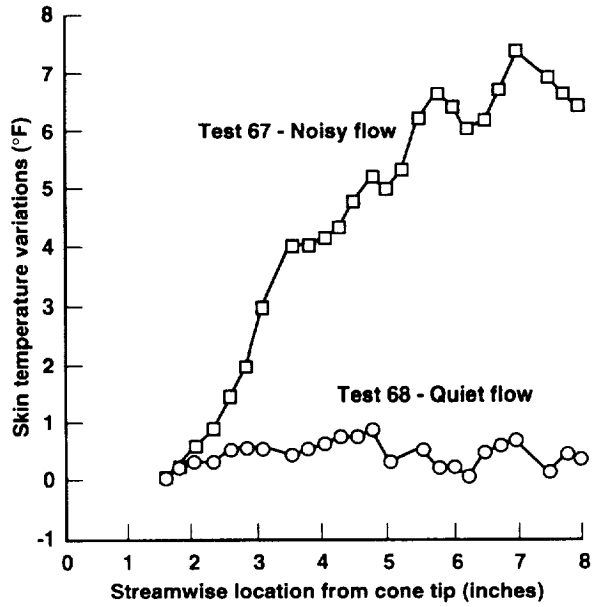

Figure 12. Comparison of 10° cone temperature distributions with noisy and quiet flow. Cone length = 15 inches (38 cm); Mach 1.586; transition free; Po = 7.5 psia; α = 0°.

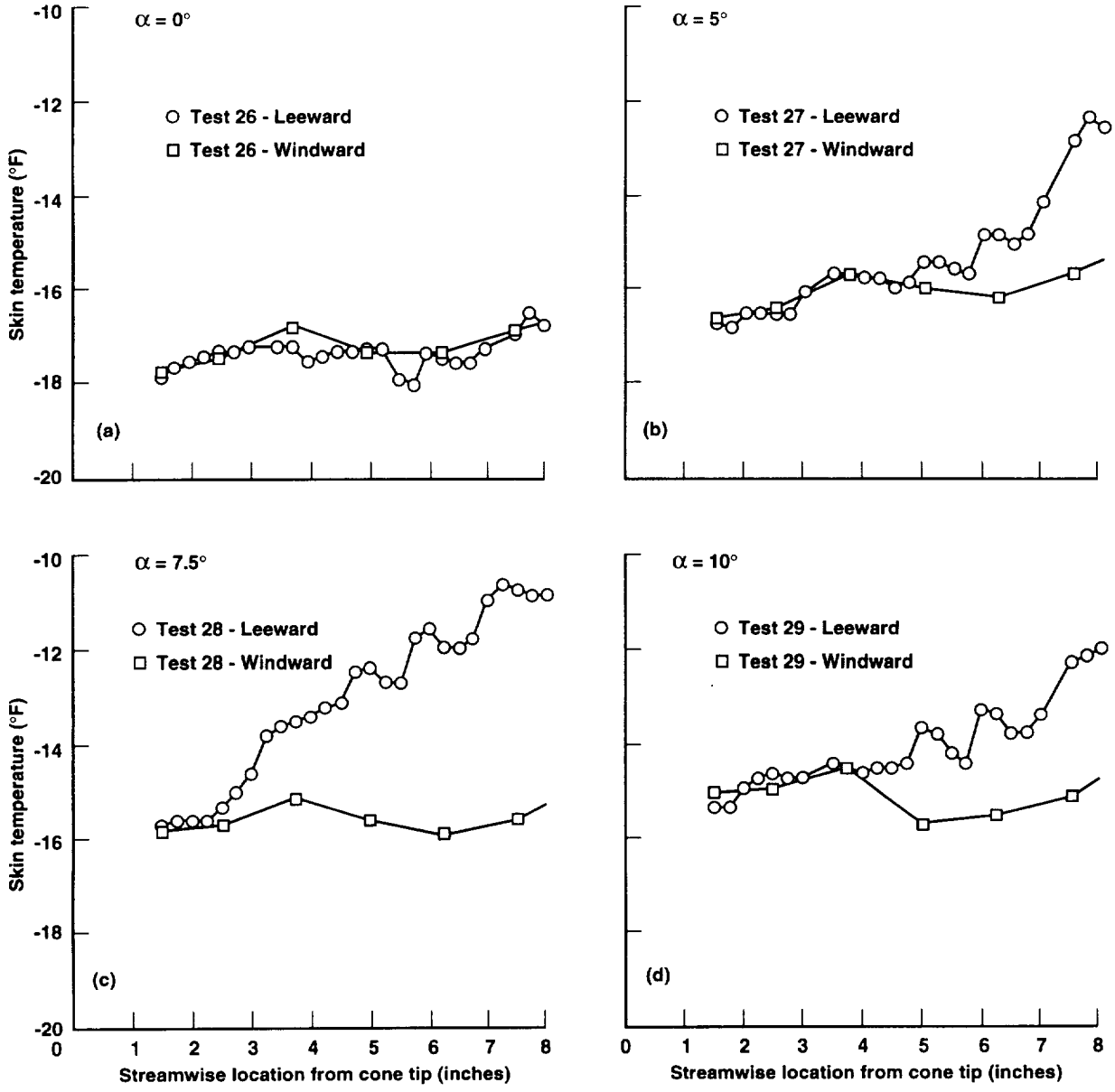

Figure 13. Cone temperature distributions on the leeward and windward sides. Cone length = 15 inches (38 cm); Mach 1.586; transition free; Po = 7.5 psia. (a) α = 0.0°; (b) α = 5.0°; (c) α = 7.5°; (d) α = 10.0°.

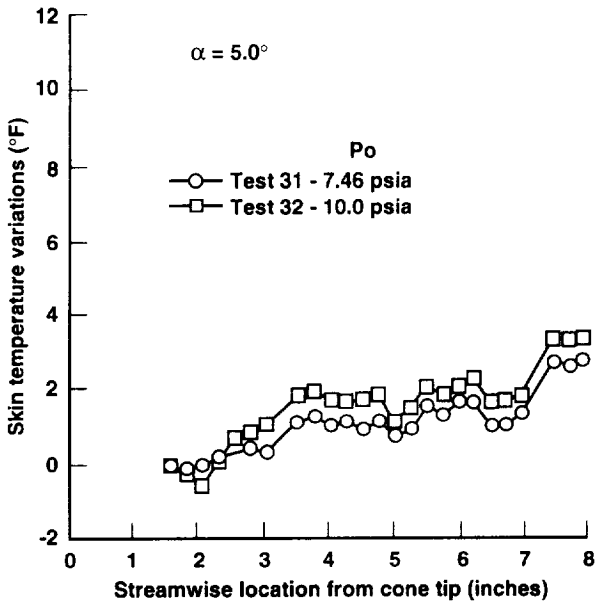

Figure 14. Effect of Reynolds number on 10° cone temperatures with transition free. Cone length = 15 inches (38 cm); Mach 1.586; α = 5°.

6. Discussion of Results

The clean cone exhibits no skin temperature rise until after the bow shock reflection impinges on the surface, over the range of Po (as shown in fig. 8). The boundary layer trip produces a repeatable initial temperature rise of order 4° F (2.2° C) as shown in figure 9. This temperature rise is very similar to that which occurs downstream of the bow shock reflection. Clearly, the trip has a profound effect on the temperature variation along the cone (as shown in fig. 10), which is indicative of the difference between laminar and turbulent boundary layers.

Oil flow interferometry was used to measure skin friction at discrete points along a cone ray, which coincided with one of the thermocouple rays. The skin friction coefficient (downstream of the trip location) is about four times larger with the trip fitted (as shown in fig. 11), and is indicative of a turbulent boundary layer. Data repeatability for this measurement technique was not demonstrated. Nevertheless, this technique offers a reasonable way of confirming the information gleaned from the skin temperature distributions. We are therefore confident that the repeatable skin temperature rise due to the trip is a consequence of transition on the cone.

When the pressure disturbances in the test section were increased by tripping the tunnel wall boundary layers, a temperature rise was observed on the cone starting near 2 inches (5.08 cm) from the cone tip (as shown in fig. 12). This temperature rise is similar to the case with the trip fitted to the cone. So we can conclude that transition was observed on the cone (within the test core) with noisy flow. At Po = 7.5 psia (0.52 bar), our CFD predictions of the transition Reynolds numbers on the cone, using e^n linear theory, were order 0.2 million in noisy flow (n = 4), and 6 million in quiet flow (n = 10). We actually observed transition only in noisy flow between 0.3 and 0.6 million. So our CFD predictions for the amplification of Tollmien-Schlichting disturbances with noisy flow were of the right order.

By varying angle of incidence, we were able to observe a transition front on the leeward side of the cone. The skin temperatures at 0°, 5°, 7.5°, and 10° with the stagnation pressure fixed at 7.5 psia (0.52 bar) (Re ~ 2.8 million per foot (9.2 million per meter)) are shown in figures 13(a), 13(b), 13(c), and 13(d) respectively. At 5° angle of attack, transition onset is shown where the associated temperature rise (with respect to the windward side) exceeds the 1° F (0.55° C) measurement resolution band. As angle of attack is increased, so the transition onset moves upstream (see fig. 13(c)). However, at 10° incidence, the difference between leeward and windward skin temperature appears to decrease, as shown in figure 13(d). We surmise that at this relatively high angle of attack, the flow may be separated on the leeward side causing unpredictable and erratic changes to the skin temperatures.

There is a similarity between the 0° and 10° temperature distributions (considering the thermocouple resolution). This finding again highlights the importance of being able to fix or move the transition onset to calibrate any transition detection technique. It can be seen that the initial temperature rise associated with the cross-flow induced transition onset is of the order 2.5° F (1.4° C). This initial temperature rise is roughly half of what we have observed at zero angle of attack with noisy flow, where Tollmien-Schlichting instabilities are dominant. The smaller initial temperature rise can be attributed to a slower transition process which occurs over a greater streamwise distance. We can surmise that the instability mechanisms causing transition affect both the initial temperature rise associated with the phenomena and the subsequent rate of temperature rise as the phenomena progress to full turbulence.

During tests with quiet (normal) flow, the skin temperature variations shown in figures 8 and 9, with and without a cone trip fitted, illustrate an insensitivity of the transition phenomena to unit Reynolds number. This may be attributed to the relatively small Re range capability of the LFSWT. Hence, small variations of Re, due to the uncontrolled variation of To, are probably not significant. In addition, there is apparently no significant effect of

small changes of unit Reynolds number on cone data at angle of attack (as shown in fig. 14 for 5° incidence). During special tests with noisy flow, only small movements of transition onset location with Re were observed, which could be attributed to data scatter.

The flight test and wind tunnel data show that transition is very sensitive to angle of incidence in the ±1° range investigated by Fisher (ref. 3). In fact, in wind tunnel tests, the transition onset was seen to shift from 11.4 inches (28.96 cm) to 7.6 inches (19.3 cm) from the tip at Mach 1.6 and Re = 3 million per foot (9.8 million per meter). In the LFSWT tests, relatively high angles of attack (>5°) were necessary to bring the transition front forward to within 8 inches (20.3 cm) of the tip, where it could be measured.

In summary, transition location on the 10° cone in the LFSWT test core (at near zero incidence) was found to be very sensitive to the state of the wall boundary layers. Also, transition location on the 10° cone in the LFSWT test core was found to be relatively insensitive to changes in angle of incidence. The proximity of the LFSWT test section walls to the model meant that the flow quality within the test core was dominated by the state of the wall boundary layers. We found that the normal flow quality in the LFSWT did not force transition within the test core, and satisfied the generally accepted low-disturbance criteria by direct measurement. Furthermore, the lack of transition within the test core up to relatively high angles of incidence indicates a similarity between the receptivity of the laminar boundary layer on the cone in the LFSWT, and that in flight. Based on these findings, we can conclude that the LFSWT flow is both low-disturbance and better than the flow encountered in the large wind tunnels used by Dougherty and Fisher. Interestingly, operating the LFSWT in a noisy mode serves as a very useful test condition for the future study of transition detection techniques at supersonic speeds.

7. Conclusions

1) A 10° cone was tested in the LFSWT at Mach 1.6, and transition measurements were made using thermocouples, oil flow interferometry, and Schlieren flow visualization.

2) Both direct and indirect flow quality measurements now indicate that the LFSWT test section flow (test core) is quiet (low-disturbance) during normal operation.

3) Transition on the cone at angle of attack, due to cross-flow instabilities, can only be measured in the test core at relatively high incidences (>5°), due to the good LFSWT flow quality.

4) Transition on the 10° cone, tested in the LFSWT, produces different skin temperature profiles depending on the type of boundary layer instability primarily responsible for the phenomena.

5) A simulated noisy tunnel environment in the LFSWT brings transition onto the cone within 2 inches (5.08 cm) of the tip, ideal for future measurement technique development at low stagnation temperatures.

6) The LFSWT cone data set is an important addition to the existing database at Mach 1.6.

Appendix

Tabulation of Selected 10° Cone Temperature Data

Skin temperature variations on a 10° cone. Mach 1.586; transition free; $\alpha = 0°$ (see fig. 8)

X location from tip	Test 68 °F	Test 69 °F	Test 70 °F
1.5	0.0	0.0	0.0
1.8	0.2	0.2	0.3
2.0	0.3	0.3	0.3
2.3	0.3	0.3	0.2
2.5	0.5	0.5	0.5
2.8	0.4	0.4	0.3
3.0	0.4	0.4	0.3
3.5	0.3	0.3	0.3
3.8	0.4	0.4	0.4
4.0	0.5	0.5	0.5
4.3	0.7	0.7	0.6
4.5	0.6	0.6	0.4
4.8	0.7	0.7	0.4
5.0	0.2	0.2	0.0
5.3	0.2	0.2	–0.1
5.5	0.5	0.5	0.2
5.8	0.2	0.2	–0.1
6.0	–0.1	–0.1	–0.1
6.3	–0.2	–0.2	–0.4
6.5	0.1	0.1	–0.2
6.8	0.2	0.2	–0.1
7.0	0.4	0.4	0.1
7.5	0.1	0.1	–0.2
7.8	0.3	0.3	0.1
8.0	0.1	0.1	–0.1
8.3	0.0	0.0	–0.2
8.5	–0.6	–0.6	
8.8	0.5	0.5	0.0
9.0	–0.2	–0.2	–0.4
9.3	0.3	0.3	0.0
9.5	0.6	0.6	0.1
9.8	1.0	1.0	0.3
10.3	1.2	1.2	0.0
10.5	2.0	2.0	0.6
10.8	2.3	2.3	0.7
11.0	3.0	3.0	1.1
11.3	3.4	3.4	1.2
11.5	4.1	4.1	1.3
11.8	4.5	4.5	1.7
12.0	4.6	4.6	2.0
12.3	4.7	4.7	2.5
12.5	5.0	5.0	3.4
12.8	5.2	5.2	3.8
13.0	5.4	5.4	3.7
13.3	6.3	6.3	4.6
13.5	5.7	5.7	4.3
13.8	5.7	5.7	4.5
14.0	6.6	6.6	5.0
14.3	6.8	6.8	5.4
14.5	7.7	7.7	7.0

Skin temperature variations on a 10° cone. Mach 1.586; transition fixed; $\alpha = 0°$ (see fig. 9)

X location from tip	Test 31 ° F	Test 32 ° F	Test 33 ° F
1.5	0.0	0.0	0.0
1.8	0.1	0.0	–0.1
2.0	0.3	0.0	0.1
2.3	0.4	0.1	0.0
2.5	0.5	0.3	0.3
2.8	0.6	0.2	0.3
3.0	0.7	0.4	0.2
3.5	0.8	0.5	0.6
3.8	1.0	0.7	0.6
4.0	1.3	1.0	1.0
4.3	1.6	1.5	1.4
4.5	2.0	2.0	1.4
4.8	2.8	2.9	2.4
5.0	5.0	3.9	3.8
5.3	5.1	3.7	4.7
5.5	4.0	4.2	4.9
5.8	5.0	4.6	4.6
6.0	5.7	5.3	5.3
6.3	5.9	5.6	5.3
6.5	6.1	5.9	5.8
6.8	6.3	5.9	5.8
7.0	6.6	6.2	6.0
7.5	6.9	6.5	6.8
7.8	6.8	6.4	6.6
8.0	6.9	6.4	6.7
8.3	6.7	6.3	6.7
8.5	6.4	5.6	6.6
8.8	6.8	6.2	6.5
9.0	6.8	6.1	6.5
9.3	6.6	5.9	6.2
9.5	6.4	6.1	6.4
9.8	6.3	6.0	6.3
10.3	6.2	5.7	6.2
10.5	6.5	6.2	6.7
10.8	6.4	5.9	6.6
11.0	6.5	6.2	6.8
11.3	6.7	6.2	6.8
11.5	6.5	6.1	6.4
11.8	6.6	6.1	6.5
12.0	6.6	6.2	6.4
12.3	6.5	6.1	6.3
12.5	6.5	6.2	6.7
12.8	6.3	5.9	6.3
13.0	6.6	6.2	6.3
13.3	6.7	6.5	6.6
13.5	6.7	6.2	6.6
13.8	7.0	6.2	6.6
14.0	7.4	6.9	7.0
14.3	7.5	6.9	7.1
14.5	8.5	8.0	8.3

Skin temperature variations on a 10° cone. Mach 1.586; transition fixed and free; $\alpha = 0°$ (see fig. 10)

X location from tip	Test 33 ° F	Test 34 ° F
1.5	0.0	0.0
1.8	–0.1	0.0
2.0	0.1	0.1
2.3	0.0	0.2
2.5	0.3	0.3
2.8	0.3	0.2
3.0	0.2	0.3
3.5	0.6	0.5
3.8	0.6	0.5
4.0	1.0	0.3
4.3	1.4	0.1
4.5	1.4	0.2
4.8	2.4	0.2
5.0	3.8	–0.3
5.3	4.7	–0.4
5.5	4.9	–0.3
5.8	4.6	–0.5
6.0	5.3	–0.4
6.3	5.3	–0.4
6.5	5.8	–0.6
6.8	5.8	–0.8
7.0	6.0	–0.5
7.5	6.8	0.4
7.8	6.6	0.2
8.0	6.7	0.2
8.3	6.7	0.3
8.5	6.6	0.2
8.8	6.5	0.1
9.0	6.5	1.4
9.3	6.2	1.3
9.5	6.4	0.0
9.8	6.3	0.0
10.3	6.2	1.4
10.5	6.7	2.4
10.8	6.6	2.4
11.0	6.8	2.7
11.3	6.8	3.0
11.5	6.4	2.2
11.8	6.5	2.5
12.0	6.4	2.6
12.3	6.3	2.8
12.5	6.7	4.4
12.8	6.3	5.1
13.0	6.3	3.2
13.3	6.6	4.6
13.5	6.6	5.9
13.8	6.6	6.3
14.0	7.0	5.8
14.3	7.1	6.1
14.5	8.3	7.8

Skin temperature variations on a 10° cone. Mach 1.586; transition free; noisy and quiet flow; $\alpha = 0°$ (see fig. 12)

X location	Test 67		Test 68		Test 55	
from tip	Temp ° F	Temp variation ° F	Temp ° F	Temp variation ° F	Temp ° F	Temp variation ° F
1.5	-20.3	0.0	-19.3	0.0	-18.1	0.0
1.8	-20.1	0.2	-19.1	0.2	-17.8	0.3
2.0	-19.7	0.6	-19.0	0.3	-17.1	1.0
2.3	-19.5	0.8	-19.0	0.3	-16.4	1.7
2.5	-18.9	1.4	-18.8	0.5	-16.0	2.1
2.8	-18.4	1.9	-18.8	0.5	-15.1	3.0
3.0	-17.3	3.0	-18.8	0.5	-14.0	4.1
3.5	-16.3	4.0	-18.9	0.4	-12.2	5.9
3.8	-16.3	4.0	-18.8	0.5	-11.7	6.4
4.0	-16.2	4.1	-18.7	0.6	-11.5	6.6
4.3	-16.0	4.3	-18.6	0.7	-11.6	6.5
4.5	-15.5	4.8	-18.6	0.7	-12.6	5.5
4.8	-15.1	5.2	-18.5	0.8	-12.8	5.3
5.0	-15.3	5.0	-19.0	0.3	-12.3	5.8
5.3	-15.0	5.3	-19.1	0.2	-11.8	6.3
5.5	-14.1	6.2	-18.8	0.5	-12.6	5.5
5.8	-13.7	6.6	-19.1	0.2	-12.6	5.5
6.0	-13.9	6.4	-19.1	0.2	-11.7	6.4
6.3	-14.3	6.0	-19.3	0.0	-12.4	5.7
6.5	-14.2	6.1	-18.9	0.4	-12.7	5.4
6.8	-13.6	6.7	-18.8	0.5	-12.6	5.5
7.0	-13.0	7.3	-18.7	0.6	-11.7	6.4
7.5	-13.4	6.9	-19.2	0.1	-12.1	6.0
7.8	-13.7	6.6	-18.9	0.4	-12.7	5.4
8.0	-13.9	6.4	-19.0	0.3	-13.3	4.8
8.3	-14.4	5.9	-19.1	0.2	-13.6	4.5
8.5	-14.2	6.1	-19.5	-0.2	-16.1	2.0
8.8	-14.1	6.2	-18.8	0.5	-13.7	4.4
9.0	-15.0	5.3	-19.7	-0.4	-13.6	4.5
9.3	-15.1	5.2	-19.3	0.0	-13.8	4.3
9.5	-14.6	5.7	-18.8	0.5	-14.7	3.4
9.8	-14.6	5.7	-18.7	0.6	-15.0	3.1
10.3	-14.2	6.1	-19.2	0.1	-13.6	4.5
10.5	-14.3	6.0	-18.8	0.5	-12.6	5.5
10.8	-14.4	5.9	-18.7	0.6	-12.6	5.5
11.0	-14.2	6.1	-18.4	0.9	-12.6	5.5
11.3	-14.0	6.3	-18.3	1.0	-12.4	5.7
11.5	-13.4	6.9	-17.9	1.4	-13.0	5.1
11.8	-13.2	7.1	-17.5	1.8	-12.5	5.6
12.0	-13.5	6.8	-17.2	2.1	-12.6	5.5
12.3	-13.7	6.6	-16.8	2.5	-12.5	5.6
12.5	-13.6	6.7	-16.3	3.0	-12.1	6.0
12.8	-13.5	6.8	-15.7	3.6	-12.2	5.9
13.0	-13.4	6.9	-15.3	4.0	-12.1	6.0
13.3	-12.9	7.4	-14.5	4.8	-11.5	6.6
13.5	-13.1	7.2	-15.2	4.1	-11.7	6.4
13.8	-13.2	7.1	-15.1	4.2	-11.2	6.9
14.0	-12.3	8.0	-14.0	5.3	-11.1	7.0
14.3	-12.1	8.2	-13.6	5.7	-11.1	7.0
14.5	-11.2	9.1	-12.2	7.1	-9.1	9.0

Skin temperature variations on a 10° cone. Mach 1.586; transition free; Po = 7.5 psia (0.52 bar) (see fig. 13)

X location	Test 26	Test 27	Test 28	Test 29	X location	Test 26	Test 27	Test 28	Test 29
leeward	$\alpha = 0°$	$\alpha = 5.0°$	$\alpha = 7.5$	$\alpha = 10°$	windward	$\alpha = 0°$	$\alpha = 5.0°$	$\alpha = 7.5°$	$\alpha = 10°$
1.5	−17.9	−16.8	−15.7	−15.3	1.5	−17.8	−16.7	−15.8	−15.0
1.8	−17.7	−16.9	−15.6	−15.3	2.5	−17.5	−16.4	−15.7	−14.9
2.0	−17.6	−16.6	−15.6	−14.9	3.8	−16.9	−15.7	−15.1	−14.5
2.3	−17.5	−16.6	−15.6	−14.7	5.0	−17.4	−16.0	−15.6	−15.7
2.5	−17.4	−16.6	−15.3	−14.6	6.3	−17.4	−16.2	−15.9	−15.5
2.8	−17.4	−16.6	−15.0	−14.7	7.5	−17.0	−15.7	−15.6	−15.1
3.0	−17.3	−16.1	−14.6	−14.7	10.0	−15.8	−14.3	−13.8	−13.2
3.5	−17.3	−15.7	−13.8	−14.4	11.3	−15.4	−14.1	−13.7	−12.8
3.8	−17.3	−15.7	−13.6	−14.5	14.0	−14.3	−12.0	−12.5	−9.9
4.0	−17.6	−15.8	−13.5	−14.6					
4.3	−17.5	−15.8	−13.4	−14.5					
4.5	−17.4	−16.0	−13.2	−14.5					
4.8	−17.4	−15.9	−13.1	−14.4					
5.0	−17.3	−15.4	−12.4	−13.6					
5.3	−17.3	−15.4	−12.3	−13.7					
5.5	−18.0	−15.6	−12.7	−14.2					
5.8	−18.1	−15.7	−12.7	−14.4					
6.0	−17.4	−14.8	−11.7	−13.2					
6.3	−17.5	−14.8	−11.5	−13.3					
6.5	−17.6	−15.0	−11.9	−13.7					
6.8	−17.6	−14.8	−11.9	−13.7					
7.0	−17.3	−14.1	−11.7	−13.3					
7.5	−17.0	−12.8	−10.9	−12.2					
7.8	−16.5	−12.3	−10.6	−12.1					
8.0	−16.8	−12.5	−10.7	−11.9					
8.3	−17.0	−12.7	−10.8	−12.0					
8.5	−20.1	−15.5	−10.8	−11.3					
8.8	−16.8	−13.1	−10.7	−12.1					
9.0	−17.4	−13.2	−10.1	−11.0					
9.3	−17.5	−13.3	−10.3	−11.0					
9.5	−17.4	−13.1	−10.7	−11.7					
9.8	−17.2	−12.9	−10.4	−11.7					
10.3	−17.3	−12.4	−9.9	−10.3					
10.5	−16.6	−11.6	−8.8	−9.1					
10.8	−16.5	−11.6	−8.9	−9.1					
11.0	−16.0	−11.1	−8.6	−8.8					
11.3	−15.9	−11.1	−8.5	−8.7					
11.5	−16.1	−11.6	−9.3	−9.8					
11.8	−15.9	−11.7	−9.5	−9.8					
12.0	−15.6	−11.7	−9.5	−9.9					
12.3	−15.4	−11.8	−9.4	−10.0					
12.5	−14.3	−10.8	−8.3	−8.4					
12.8	−13.7	−10.9	−8.6	−8.6					
13.0	−14.3	−11.6	−9.5	−10.2					
13.3	−13.3	−11.2	−9.1	−9.9					
13.5	−12.7	−10.5	−8.1	−8.4					
13.8	−12.7	−10.7	−8.3	−8.5					
14.0	−12.2	−11.0	−9.0	−9.7					
14.3	−11.8	−10.8	−8.8	−9.6					
14.5	−10.7	−9.3	−7.6	−8.1					

Skin temperatures on a 10° cone. Mach 1.586; transition free; $\alpha = 5.0°$ (see fig. 14)

X location	Test 31		Test 32	
from tip	Skin temp ° F	Temp variation ° F	Skin Temp ° F	Temp variation ° F
1.5	−16.7	0.0	−17.3	0.0
1.8	−16.6	0.1	−17.3	0.0
2.0	−16.4	0.3	−17.3	0.0
2.3	−16.3	0.4	−17.2	0.1
2.5	−16.2	0.5	−17.0	0.3
2.8	−16.1	0.6	−17.1	0.2
3.0	−16.0	0.7	−16.9	0.4
3.5	−15.9	0.8	−16.8	0.5
3.8	−15.7	1.0	−16.6	0.7
4.0	−15.4	1.3	−16.3	1.0
4.3	−15.1	1.6	−15.8	1.5
4.5	−14.7	2.0	−15.3	2.0
4.8	−13.9	2.8	−14.4	2.9
5.0	−11.7	5.0	−13.4	3.9
5.3	−11.6	5.1	−13.6	3.7
5.5	−12.7	4.0	−13.1	4.2
5.8	−11.7	5.0	−12.7	4.6
6.0	−11.0	5.7	−12.0	5.3
6.3	−10.8	5.9	−11.7	5.6
6.5	−10.6	6.1	−11.4	5.9
6.8	−10.4	6.3	−11.4	5.9
7.0	−10.1	6.6	−11.1	6.2
7.5	−9.8	6.9	−10.8	6.5
7.8	−9.9	6.8	−10.9	6.4
8.0	−9.8	6.9	−10.9	6.4
8.3	−10.0	6.7	−11.0	6.3
8.5	−10.3	6.4	−11.7	5.6
8.8	−9.9	6.8	−11.1	6.2
9.0	−9.9	6.8	−11.2	6.1
9.3	−10.1	6.6	−11.4	5.9
9.5	−10.3	6.4	−11.2	6.1
9.8	−10.4	6.3	−11.3	6.0
10.3	−10.5	6.2	−11.6	5.7
10.5	−10.2	6.5	−11.1	6.2
10.8	−10.3	6.4	−11.4	5.9
11.0	−10.2	6.5	−11.1	6.2
11.3	−10.0	6.7	−11.1	6.2
11.5	−10.2	6.5	−11.2	6.1
11.8	−10.1	6.6	−11.2	6.1
12.0	−10.1	6.6	−11.1	6.2
12.3	−10.2	6.5	−11.2	6.1
12.5	−10.2	6.5	−11.1	6.2
12.8	−10.4	6.3	−11.4	5.9
13.0	−10.1	6.6	−11.1	6.2
13.3	−10.0	6.7	−10.8	6.5
13.5	−10.0	6.7	−11.1	6.2
13.8	−9.7	7.0	−11.1	6.2
14.0	−9.3	7.4	−10.4	6.9
14.3	−9.2	7.5	−10.4	6.9
14.5	−8.2	8.5	−9.3	8.0

References

1. Dougherty, N. S.; and Fisher, D. F.: Boundary Layer Transition on a 10-Degree Cone: Wind Tunnel/ Flight Data Correlation. AIAA Paper 80-0154. Invited paper presented at the 18th AIAA Aerospace Sciences Meeting, Pasadena, Calif., Jan. 1980, 16 p.

2. Dougherty, N. S.: Influence of Wind Tunnel Noise on Location of Boundary-Layer Transition on a Slender Cone at Mach Numbers from 0.2 to 5.5 – Final Report 1970-7. AEDC-TR-78-44, Mar. 1980, 246 p.

3. Fisher, D. F.; and Dougherty, N. S.: In-Flight Transition Measurement on a 10° Cone at Mach Numbers from 0.5 to 2.0. NASA TP-1971, June 1982. 143 p.

4. Wolf, S. W. D.; Laub, J. A.; and King, L. S.: Flow Characteristics of the NASA-Ames Laminar Flow Supersonic Wind Tunnel for Mach 1.6 Operation. AIAA Paper 94-2502. Invited paper presented at the 18th AIAA Aerospace Ground Testing Conference, Colorado Springs, Colo., June 1994, 18 p.

5. Westley, R.: Problems of Noise Measurement in Ground Based Facilities with Forward-Speed Simulation (High Speed Wind Tunnel Noise). In: A Further Review of Current Research Aimed at the Design and Operation of Large Wind Tunnels – Appendix 5, AGARD AR-83, Sept. 1975, pp. 75–100.

6. Wolf, S. W. D.; and Laub, J. A.: Low-Disturbance Flow Measurements in the NASA-Ames Laminar Flow Supersonic Wind Tunnel. AIAA Paper 96-2189. Presented at the 19th AIAA Advanced Measurement and Ground Testing Technology Conference, New Orleans, La., June 1996, 19 p.

7. Wolf, S. W. D.; and Laub, J. A.: Characteristics of the NASA-Ames Laminar Flow Supersonic Wind Tunnel for Unique Mach 1.6 Transition Studies. In: Conference Proceedings of the 79th AGARD-FDP Symposium on Aerodynamics of Wind Tunnels and Their Components, Moscow, Russia, Sept.–Oct. 1996, pp. 30-1 – 30-17.

8. Morris, D. E.; and Winter, K. G.: Requirements for Uniformity of Flow in Supersonic Wind Tunnels. RAE TN Aero. 2340, Sept. 1954.

9. Zilliac, G. G: Further Developments of the Fringe-Imaging Skin Friction Technique. NASA TM-110425, Dec. 1996, 38 p.

REPORT DOCUMENTATION PAGE

Form Approved
OMB No. 0704-0188

1. AGENCY USE ONLY *(Leave blank)*	2. REPORT DATE	3. REPORT TYPE AND DATES COVERED
	March 1997	Technical Memorandum

4. TITLE AND SUBTITLE

NASA Ames Laminar Flow Supersonic Wind Tunnel (LFSWT) Tests of a 10° Cone at Mach 1.6

5. FUNDING NUMBERS

537-03-23

6. AUTHOR(S)

Stephen W. D. Wolf* and James A. Laub

7. PERFORMING ORGANIZATION NAME(S) AND ADDRESS(ES)

Ames Research Center
Moffett Field, CA 94035-1000

8. PERFORMING ORGANIZATION REPORT NUMBER

A-976108

9. SPONSORING/MONITORING AGENCY NAME(S) AND ADDRESS(ES)

National Aeronautics and Space Administration
Washington, DC 20546-0001

10. SPONSORING/MONITORING AGENCY REPORT NUMBER

NASA TM-110438

11. SUPPLEMENTARY NOTES

Point of Contact: Stephen W. D. Wolf, Ames Research Center, MS 260-1, Moffett Field, CA 94035-1000
(415) 604-1202
*MCAT, Inc., 3933 Blue Gum Dr., San Jose, CA 95127

12a. DISTRIBUTION/AVAILABILITY STATEMENT

Unclassified — Unlimited
Subject Category 09, 02

12b. DISTRIBUTION CODE

13. ABSTRACT ***(Maximum 200 words)***

This work is part of the ongoing qualification of the NASA Ames Laminar Flow Supersonic Wind Tunnel (LFSWT) as a low-disturbance (quiet) facility suitable for transition research. A 10° cone was tested over a range of unit Reynolds numbers (Re = 2.8 to 3.8 million per foot (9.2 to 12.5 million per meter)) and angles of incidence (0° to 10°) at Mach 1.6. The location of boundary layer transition along the cone was measured primarily from surface temperature distributions, with oil flow interferometry and Schlieren flow visualization providing confirmation measurements. With the LFSWT in its normal quiet operating mode, no transition was detected on the cone in the test core, over the Reynolds number range tested at zero incidence and yaw. Increasing the pressure disturbance levels in the LFSWT test section by a factor of five caused transition onset on the cone within the test core, at zero incidence and yaw. When operating the LFSWT in its normal quiet mode, transition could only be detected in the test core when high angles of incidence (>5°) for cones were set. Transition due to elevated pressure disturbances (Tollmien-Schlichting) and surface trips produced a skin temperature rise of order 4° F (2.2° C). Transition due to cross flows on the leeward side of the cone at incidence produced a smaller initial temperature rise of only order 2.5° F (1.4° C), which indicates a slower transition process. We can conclude that these cone tests add further proof that the LFSWT test core is normally low-disturbance (pressure fluctuations > 0.1%), as found by associated direct flow quality measurements discussed in this report. Furthermore, in a quiet test environment, the skin temperature rise is sensitive to the type of dominant instability causing transition. The testing of a cone in the LFSWT provides an excellent experiment for the development of advanced transition detection techniques.

14. SUBJECT TERMS	15. NUMBER OF PAGES
Laminar flow, Supersonic, Cone test	23
	16. PRICE CODE: A03

17. SECURITY CLASSIFICATION OF REPORT	18. SECURITY CLASSIFICATION OF THIS PAGE	19. SECURITY CLASSIFICATION OF ABSTRACT	20. LIMITATION OF ABSTRACT
Unclassified	Unclassified		